Task-Based Optimization of Source-Detector Orbits in Interventional Cone-beam CT

J. Webster Stayman, Grace J. Gang, and Jeffrey H. Siewerdsen

***Abstract*—In this paper a methodology for task-based optimization of source-detector orbits is presented. The design process is aligned well with an interventional workflow where preoperative imaging is available to provide patient-specific anatomical information, where the imaging task is well-defined, and there exist interventional imaging devices (e.g., robotic C-arms) that are capable of sophisticated source-detector trajectories. The proposed orbital optimization is based on an objective function that uses task-based detectability as the performance metric. Nonconvex optimization (CMA-ES) is used to estimate design solutions. This framework is tested in some simple imaging scenarios to illustrate the importance of task location as well as the particular imaging task function. More complex experiments are conducted on an emulated postoperative assessment of a coil embolization of an intracranial aneurysm. The improved performance for designed orbits over traditional circular orbits is illustrated and discussed.**

***Index Terms*—Task-based assessment, human observer models, adaptive imaging, robotic C-arms, image quality.**

I. Introduction

Interventional cone-beam CT systems are finding increased application in many minimally invasive procedures. For example, 3D-capable C-arm systems can provide up-to-date anatomical information throughout an intervention and can be used at the conclusion of a procedure for post-operative assessment. The workflow and diagnostic aims in interventional imaging provide an excellent opportunity to customize acquisitions to the specific patient and task for a number of reasons: Interventional imaging: 1) is nearly always preceded by diagnostic imaging providing a rich source of patient-specific anatomical knowledge that can be leveraged for acquisition optimization; 2) is often focused on well-defined and localized imaging tasks (e.g., bleed detection at the site of the intervention) that can modeled and used for performance prediction; and 3) often suffers from reduced data fidelity relative to traditional diagnostic imaging, and could benefit from image quality improvements.

Consider the workflow in Figure 1 for an endovascular embolization of an intracranial aneurysm. Preoperative images are used to determine the amount of embolization coil required, the need for a stent, etc. Locations of interest and particular imaging tasks can often be defined. For example, the detection of bleeds or perforations of the aneurysm are well-defined in location (i.e., near the aneurysm) with known characteristics (i.e., contrast, general shape of a bleed, etc.). Conventional intraoperative 3D imaging disregards this prior information – typically restricting acquisitions to a circular orbit and often suffering from poor image quality in the vicinity of the embolization coil which is precisely where bleed detection needs to be performed. We choose to leverage prior information about the patient anatomy and coil embolization plan to design source-detector trajectories customized to the patient and imaging task.

Such customization requires accurate prediction of task performance which has been successfully applied using mathematical human observer models in imaging system design and optimization. [1] Recent work has applied the same methodology to customize current modulation and reconstruction parameters for specific patients and tasks [2] and there are other examples of acquisition optimization in nuclear imaging [3] In this work, we consider acquisition design for robotic C-arm systems that are capable of arbitrary source and detector positions around the patient. We use a task performance prediction framework based on a nonprewhitening observer model to design a source-detector trajectory for specific detection tasks. Previous work attempted to solve this optimization task using a greedy algorithm based on the maximization of marginal detectability with the addition of successive single projection views. [4] While that approach is computationally tractable, it is susceptible to local minimum and poorly suited to optimization objectives with multiple tasks or multiple task locations. In this paper, we illustrate an optimization strategy that uses a low-dimensional parameterization of the orbit and nonconvex optimization of a task-based objective function that includes one or more task functions or task locations.

II. Methods

A. Workflow for Task- and Patient-Specific Acquisitions

The workflow in interventional imaging provides a rich source of information that may be used for acquisition design. Consider a typical interventional imaging workflow as illustrated in Figure 1. Initial diagnostic imaging is conducted to localize and plan a treatment procedure. Intraoperative CT is often conducted post-procedure for assessment and complication detection. We propose to use the preoperative study (as well as planning

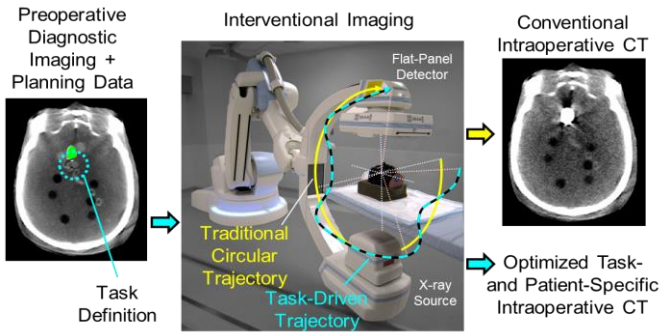

Figure 1: Illustration of the workflow in interventional imaging. Preoperative imaging is used for diagnosis and surgical planning, whereas intraoperative imaging is used to assess the procedure and detect complications. Robotic C-arms have the potential to customize their acquisition through modification of the orbit to improve image quality and/or reduce radiation exposure. We propose to inform the orbit optimization process using preoperative anatomical data possibly augmented by planning data (e.g., the size and location of an implant or tool or in the above example, an embolization coil).

This work was supported in part by NIH Grant No. U01EB018758.

J. Webster Stayman is with the Department of Biomedical Engineering, Johns Hopkins University, Baltimore, MD 21212 USA (phone: 410-955-1314; fax: 410-955-1115; e-mail: web.stayman@jhu.edu).

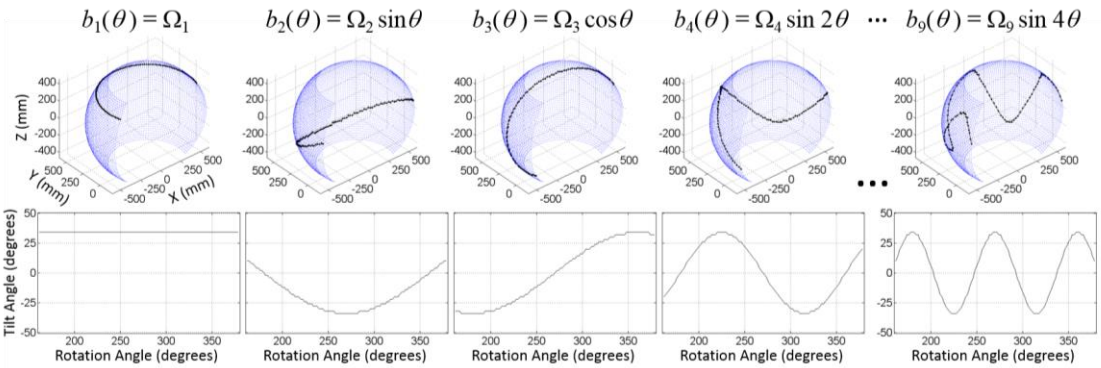

Figure 2. Illustration of a short scan orbit (top: showing source position; bottom: showing tilt angle of the gantry as a function of rotation angle) parameterized by a constant, sine, and cosine basis functions. The linear combination of these orbital bases permits a wide range of orbits. In our studies we add an additional constraint so that the maximum angular tilt is clipped at ±50°.

information) to optimize the intraoperative acquisition. In the case of a robotically controlled C-arm, we can break free from standard circular or spiral orbits to achieve more arbitrary source-detector positions. The goal is to use this flexibility in the acquisition to improve imaging performance for specific tasks. We hypothesize that there are many scenarios where such a task- and patient specific acquisition will improve performance.

B. Imaging System Model and Reconstruction

To begin, we require a system model parameterized by the acquisition values that may be varied. This model is important both for the optimization as well as the reconstruction. We choose the following mean measurement model for a CT device capable of arbitrary projection views:

$$\bar{y}_i = g_i \exp\left(\left[\mathbf{A}(\Omega)\mu\right]_i\right) \tag{1}$$

where subscript denotes the i^{th} measurement, g is a gain term that includes detector fluence and detector sensitivities, μ is a vector representing a volume of attenuation values, and the system matrix, $\mathbf{A}$, defines the projection operation for all views. We note that $\mathbf{A}$ is a function of the vector Ω which parameterizes a specific orbit and the corresponding projection views.

While (1) is completely general, in this paper, we focus on a parameterization of source and detector positions in the following fashion. First, we presume that the spatial relationship between the source and detector is preserved for all views (e.g., they are rigidly fixed to each other). Second, we presume that the center point between the source and detector is fixed spatially. This means the remaining degrees of freedom are completely specified by two angles – the usual rotation angle (θ) and a tilt angle (ρ). We choose a low-dimensional parameterization of this space presuming θ covers a specific angular range (e.g. a short scan, 360°, etc.) and ρ is a function of θ, and using a sines and cosines basis set as shown in Figure 2. The coefficient (Ω_n) of each basis function (b_n) is an element of Ω, and the orbital trajectory is defined as the sum of all weighted bases. Additionally, we clip the tilt angle to a limited range to enforce physical constraints (e.g. collision of the gantry with the patient or imaging table.)

The projection data arising from the possible generalized orbits that span the basis set in Figure 2, need to be reconstructed. Toward this end, we integrate the forward model of (1) into a penalized-likelihood approach:

$$\hat{\mu} = \arg\max_{\mu} L(\mu; y) - \beta R(\mu) \tag{2}$$

where L denotes the log-likelihood data consistency term arising from an independent Poisson noise assumption, and $R(\mu) = \mu^T\mathbf{R}\mu$ is a quadratic penalty. This widely used estimator is convenient since there are various optimizers available including the OS-SPS algorithm used here; and because (2) will provide reconstructions for arbitrary geometries as long as the routines for projection and backprojection are available.

C. Task-based Orbital Design Objective

Our orbital design seeks to maximize task performance using a human observer model. While various models exist, we choose to use detectability index based on a nonprewhitening observer model. This model may be written:

$$d_j'^2 = \frac{\left[\iiint \left(MTF_j \cdot W_{Task}\right)^2 df_x df_y df_z\right]^2}{\iiint NPS_j \cdot \left(MTF_j \cdot W_{Task}\right)^2 df_x df_y df_z} \tag{3}$$

where MTF_j denotes the (spatially) local modulation transfer function, NPS_j is the local noise power spectrum, and W_{Task} is the so-called task function that specifies the spatial frequencies of interest for the specific imaging task. (This function can be formed by taking the Fourier transform of the signal present and signal absent hypotheses.) While MTF_j and NPS_j are necessarily dependent on the location j, predictors for these functions have been derived and applied to obtain accurate estimates [5,6]. Using Fourier methods, one may estimate these functions as

$$MTF_j = \frac{\mathcal{F}\left\{\mathbf{A}^T\mathbf{D}\left\{\bar{y}(\mu)\right\}\mathbf{A}e_j\right\}}{\mathcal{F}\left\{\mathbf{A}^T\mathbf{D}\left\{\bar{y}(\mu)\right\}\mathbf{A}e_j + \beta\mathbf{R}e_j\right\}}$$
$$NPS_j = \frac{\mathcal{F}\left\{\mathbf{A}^T\mathbf{D}\left\{\bar{y}(\mu)\right\}\mathbf{A}e_j\right\}}{\left|\mathcal{F}\left\{\mathbf{A}^T\mathbf{D}\left\{\bar{y}(\mu)\right\}\mathbf{A}e_j + \beta\mathbf{R}e_j\right\}\right|^2} \tag{4}$$

where the preoperative image volume may be used as μ. While not discussed here in detail, one may recognize that the important quantity $\mathbf{A}^T\mathbf{D}\{x\}\mathbf{A}$ is linear in x, and thus a linear operator may be used (as in [7]) for fast repeated calculations.

With the relationship between task, patient anatomy, and acquisition parameters complete, we may now write our design objective:

$$\hat{\Omega} = \arg\max_{\Omega}\left(\min\left\{\begin{matrix} d_1'^2\left(\Omega; W_{Task(1)}\right), d_2'^2\left(\Omega; W_{Task(2)}\right), \\ \ldots, d_L'^2\left(\Omega; W_{Task(L)}\right)\end{matrix}\right\}\right) \tag{5}$$

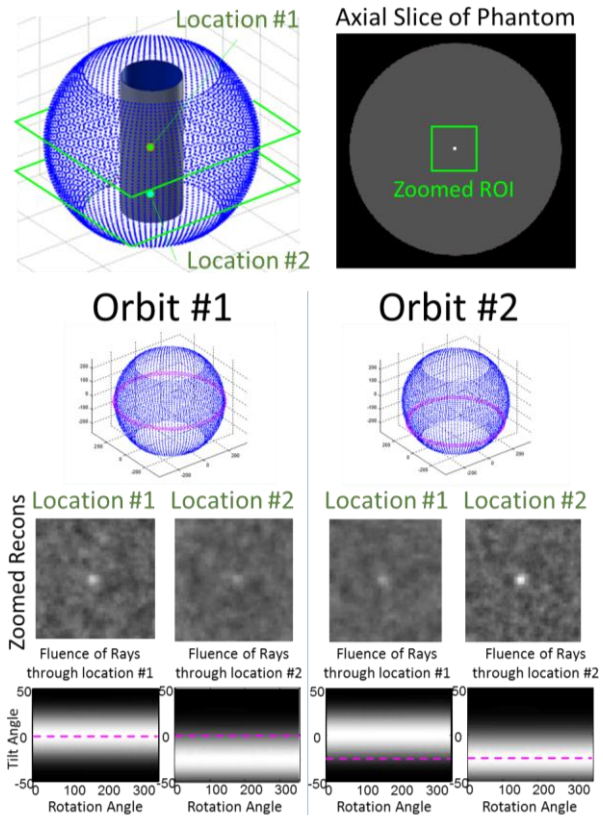

Figure 3: Separate orbital designs are performed at two locations for a point detection task (orbits indicated in magenta). In each position, the solution is the orbit that maximizes detected fluence (bottom row). While the optimal orbit for one location improves detectability for that location, the detectability for the other location is reduced.

This objective seeks to maximize the minimum detectability over L locations and/or task functions. In effect, guaranteeing a specific detectability for those positions and/or imaging tasks. For a single location/task the inner minimum disappears and the problem reduces to a "simple" maximization. Because (5) is nonconvex, we use the CMA-ES [8] algorithm to estimate a global optima.

D. Experimental Methods

We apply the design method represented by (5) a few illustrative examples. First, we consider the important of location dependence in a simple cylinder object with a high-frequency imaging task (detection of a small high-contrast point). Two orbital designs are computed for different stimulus positions and the relative detectability for the two designs and positions are compared. A second study investigates the dependence on the task function using the same cylindrical object. However, in this case, orbital designs are performed for two different task functions: 1) the symmetric high-frequency "point" task; and 2) an asymmetric task based on oriented line pairs. The resulting symmetric design (orbit S) is compared with the asymmetric design (orbit A). For both of these studies a highly attenuating cylinder (μ=0.05 mm^{-1}, 10 cm radius) was used to exaggerate spatial dependence.

The design methodology was tested on data emulating an intracranial aneurysm embolization in both physical CBCT phantom data as well as in simulation studies. While both methods explore the multi-location aspect of the objective in (5), the physical experiments are focused on a relatively compact set

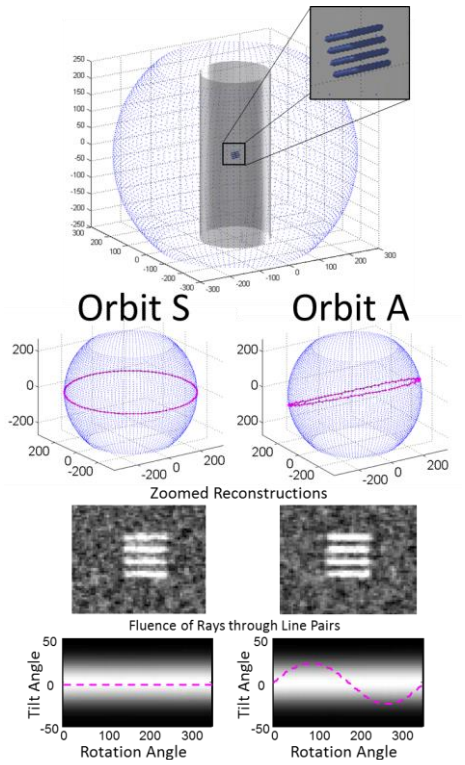

Figure 4: Task-based orbits for a symmetric point task (Orbit S), and an asymmetric task based on a line pair detection target (Orbit A) differ substantial. While Orbit S again seeks to maximize fluence through the object, Orbit A is aligned to shoot views parallel to the line pairs. The consequent improvement in detectability is apparent in the sagittal view with better separation of the lines.

of locations whereas the simulation experiments consider a more extended task area. In both cases, the task function was matched to a bleed detection task (i.e., a sphere of known contrast).

III. Results/Discussion

The location-dependence experiment is summarized in Figure 3. Orbits designed for point detection at the central slice and a slice toward the lower extreme were estimated. In each case, the optimal design was an intuitive orbit where detected fluence was maximized for the stimulus location. The location for which the orbit was *not* optimized suffers from decreased detectability due largely to the lower fluence observed by rays passing through that location (see bottom row of fluence plots).

In Figure 4, we modify the phantom slightly to have a set of line pairs at the central slice and orbits are designed for a symmetric point task (Orbit S) and an asymmetric line-pair detection task (Orbit A). The symmetric orbit duplicates the previous central slice design maximizing detector fluence. However, the asymmetric task function lead to a different design where detected fluence maximization is not optimal. In this case, detectability is maximized when Orbit A is obtaining projections that provide parallel ("through the slits") views of the line pair location. The differing performance of these two orbits is apparent in sagittal views showing increased blur between line pairs in Orbit S over the more optimal Orbit A.

The imaging results for the CBCT testbench investigation of an emulated intracranial embolization procedure are illustrated in Figure 5. Two orbits are used: 1) a standard circular trajectory, and 2) a task-driven design based on preoperative image data,

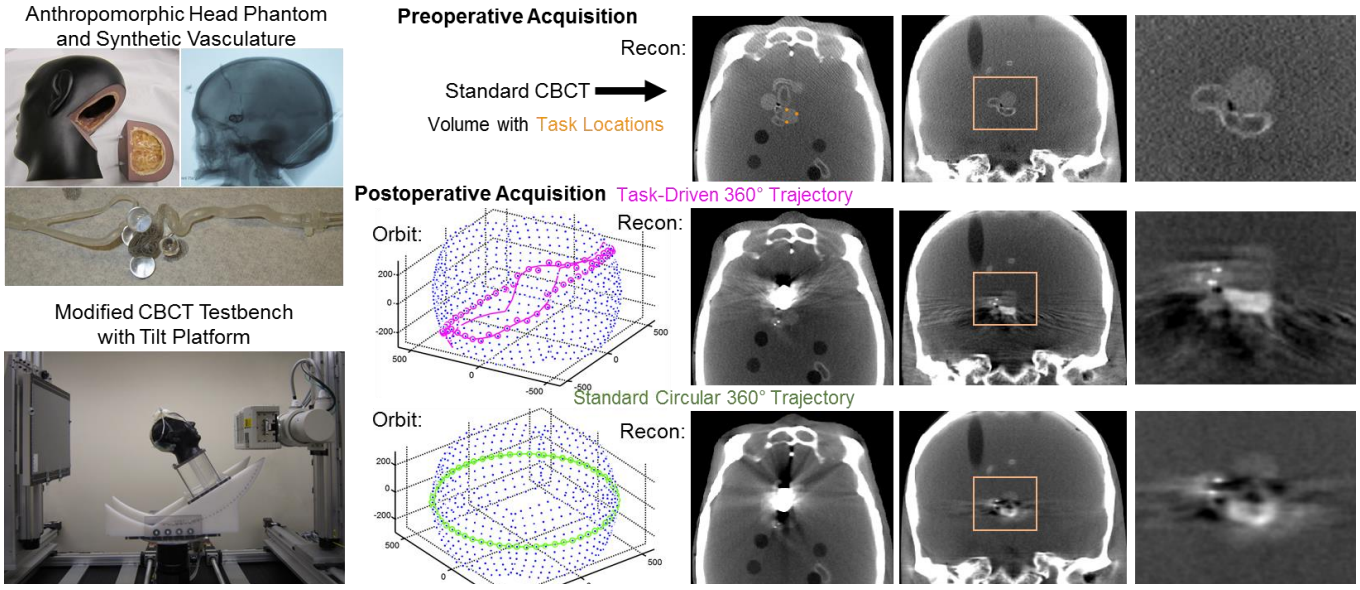

Figure 5: An emulated intracranial aneurysm imaging experiment using a custom phantom and CBCT testbench with manual tilt settings. The phantom is imaged preoperatively (top row) and postoperatively after coil embolization using a standard circular orbit (bottom row) and a task-driven orbit (middle row). Improved detectability of a simulated bleed (also present preoperatively) are improved, as is the appearance of the legs of a stent and residual iodine contrast in the synthetic vasculature (see coronal zooms).

three task locations inferior to the aneurysm, and a task function matched to the spherical bleed and contrast present in the phantom. The optimized design has a significant gantry tilt and also "wobbles" around some high attenuation structures in the head. As compared with the circular orbit visualization of the bleed is more apparent, as are the legs of a stent used to keep the coil in place and residual contrast in the synthetic vasculature.

In the last investigation, the multiple location aspect of (5) is used and summarized in Figure 6. A spherical bleed task function and a ring of locations around the embolization coil is selected in one axial slice. The resulting orbital design is unusual, cycling back-and-forth between tilt extremes (in an attempt to minimize coil overlap with the stimuli locations in the projections). Again the designed orbit outperforms a circular orbit with poor visualization only extremely close to the coil.

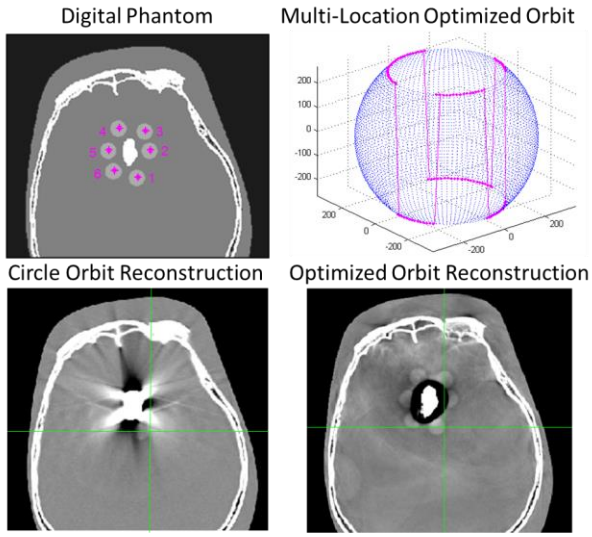

Figure 6: Illustration of a distributed multi-location optimization for six different potential bleed locations. The multi-location orbit permits visualization of bleeds near the embolization coil while the poor image quality for the circular orbit reconstruction makes visualization of bleeds difficult near the coil. (Note there is only one bleed, near the crosshairs in the circular orbit image.)

In summary, the orbital design process is capable of significant image quality improvements. The framework is general and can be extended to other acquisition parameters including other degrees of freedom and exposure modulations, permitting more widespread application of the approach on interventional system less advanced than a robotic C-arm as well as other (non-interventional) sequential imaging applications.

REFERENCES

[1]P. Prakash et al., "Task-based modeling and optimization of a cone-beam CT scanner for MSK imaging," *Med. Phys.*, vol. 38, no. 10, pp. 5612–29, Oct. 2011.

[2]G. J. Gang, J. W. Stayman, S. Ouadah, T. Ehtiati, and J. H. Siewerdsen, "Task-driven imaging in cone-beam computed tomography," in *SPIE Medical Imaging*, 2015.

[3]H. H. Barrett, L. R. Furenlid, M. Freed, J. Y. Hesterman, M. A. Kupinski, E. Clarkson, and M. K. Whitaker, "Adaptive SPECT," *IEEE Trans. Med. Imaging*, vol. 27, no. 6, pp. 775–88, Jun. 2008.

[4]J. W. Stayman and J. H. Siewerdsen, "Task-based trajectories in iterative reconstructed interventional cone-beam CT," in *Int'l Mtg. on Fully 3D Image Reconstruction in Radiology and Nuclear Medicine*, 2013, pp. 257–60.

[5]J. A. Fessler and W. L. Rogers, "Spatial resolution properties of penalized-likelihood image reconstruction: space-invariant tomographs," *IEEE Trans. Image Process.*, vol. 5, no. 9, pp. 1346–58, Jan. 1996.

[6]G. J. Gang, J. W. Stayman, W. Zbijewski, and J. H. Siewerdsen, "Task-based detectability in CT image reconstruction by filtered backprojection and penalized likelihood estimation," *Med. Phys.*, vol. 41, no. 8, p. 081902, Aug. 2014.

[7]J. W. Stayman and J. A. Fessler, "Efficient Calculation of Resolution and Covariance for Penalized-Likelihood Reconstruction in Fully 3-D SPECT," *IEEE Trans. Med. Imaging*, vol. 23, no. 12, pp. 1543–56, 2004.

[8]N. Hansen and S. Kern, "Evaluating the CMA evolution strategy on multimodal test functions," in *Parallel Problem Solving from Nature - PPSN VIII*, 2004, pp. 282–91.